Magnetophotocurrent in Organic Bulk Heterojunction Photovoltaic Cells at Low Temperatures and High Magnetic Fields

B. Khachatryan,[1] A. H. Devir-Wolfman,[1] L. Tzabari,[2] N. Tessler,[2] Z. V. Vardeny,[3] and E. Ehrenfreund[1,*]

[1]*Physics Department and Solid State Institute, Technion-Israel Institute of Technology, Haifa 32000, Israel*

[2]*Department of Electrical and Computer Engineering, Technion-Israel Institute of Technology, Haifa 32000, Israel*

[3]*Department of Physics & Astronomy, University of Utah, Salt Lake City, Utah 84112, USA*

(Received 17 November 2015; revised manuscript received 13 February 2016; published 1 April 2016)

We study high-field (up to $B \sim 8.5$ T) magnetophotocurrent (MPC) related to photogenerated polaron pairs (PPs) in the temperature range $T = 10$–320 K in organic bulk heterojunction photovoltaic cells. We find that in the high-field regime ($B > 1$ T), MPC(B) response increases with B for temperature $T > 200$ K but decreases with B at $T < 200$ K. MPC(B) response does not saturate even at the highest field studied, at all T. We attribute the observed high-field MPC(B) response to two competing mechanisms within the PP spin states: (a) a spin-mixing mechanism caused by the difference in the donor-acceptor (or positive-negative polarons) g factors (the so-called "Δg mechanism"), and (b) the spin polarization induced by thermal population of the PP Zeeman split levels. The nonsaturating MPC(B) response at high fields and high temperatures indicates that there exist charge-transfer excitons (CTEs) with decay time in the subnanosecond time domain. With decreasing temperature, the CTE decay time sharply increases, thereby promoting an increase of the thermal spin-polarization contribution to the MPC(B) response.

DOI: 10.1103/PhysRevApplied.5.044001

I. INTRODUCTION

Electronic devices in which the active layer is made of low-mobility organic semiconductors (OSECs) have recently been shown to respond substantially to relatively low magnetic fields ($B < 0.1$ T) [1–8]. The low magnetic field (B) response has been attributed to mechanisms that involve the carrier's spin rather than magnetostatic effects due to the magnetism of the extremely small electric current. In nonmagnetic OSECs in which the carrier mobility is spin independent at $B = 0$, the magnetic response is caused by the spin interaction of spin-coupled pairs that influence the device output response as a function of B [8–10]. Among the various mechanisms used to interpret the magnetic field effects on OSEC films and devices, we emphasize few that are relevant to the present work: (a) spin mixing by the hyperfine (HF) interaction within polaron pairs (PPs) and bipolarons [8,10–13], (b) the difference Δg in the electron and hole g factors that constitute the spin pair [14–18], and (c) spin polarization due to thermal population of the Zeeman split levels of the spin pair [19]. It is important to note that the outcome of the interaction using any of the proposed mechanisms must be spin dependent; e.g., the dissociation rate of a PP into positive and negative free carriers depends on its spin configuration; this is discussed in more detail below.

The power conversion efficiency (PCE) of the best organic photovoltaic (OPV) cells has reached values of approximately 10%. In OPV cells, the photoexcited singlet exciton (SE) may ionize into free carriers that contribute to the photocurrent via several intermediate processes. These processes include ultrafast transfer into charge-transfer excitons (CTEs), followed by a slower separation into correlated PPs, which dissociate into free polarons in a much slower process. The cell PCE depends critically on the recombination and dissociation of these intermediate species [20], which, in turn, depend on their spin configuration [20–22]. For example, OPV cells with spin-½ additives showed higher photocurrent than those without these ferromagnetic additives [23]. Consequently, understanding the spin physics of OPV cells may lead to better devices with higher PCE. Studying the weak and strong magnetic field effects on the photocurrent at high and low temperatures may provide comprehensive understanding of the relevant spin interactions that determine charge generation and recombination mechanisms.

In the present paper, we report on the magnetophotoconductivity (MPC) response in various bulk heterojunction OPV cells made of a polymer donor (D) and fullerene acceptor (A) subjected to a magnetic field in the range up to $B \sim 8.5$ T and temperature range $T = 10$–320 K. At all temperatures, we find that the MPC(B) response does not saturate at high B. At the higher-temperature range, we identify the main mechanism responsible for the nonsaturated behavior at high fields to be spin mixing caused by the

*Corresponding author.
eitane@technion.ac.il

difference Δg of the donor-acceptor g factors of short-lived CTEs. At low temperatures, we propose that thermal spin polarization becomes more dominant, giving rise to sign reversal of the high-field MPC(B) response. We also find that the high-field MPC(B) response shows a device- and temperature-dependent Cole-Cole dispersive profile that indicates a broad distribution of species lifetimes.

II. EXPERIMENT

A solvent-cast layer of regioregular poly(3-hexylthiophene) (rrP3HT) organic donor and 1-[3-(methoxycarbonyl)propyl]-1-1-phenyl) [6,6] C_{60} (PCBM) acceptor blend (1:1 weight ratio) is sandwiched between the cathode (30-nm Ca covered by 100-nm Al and 30-nm Au film) and the transparent anode (film of indium tin oxide, ITO) through which the active layer is photoexcited; the general structure of the OPV cells used here is shown in Fig. 1 (inset). This *D-A* blend is known to form bulk heterojunction (BHJ) of nanosized domains that facilitate charge photogeneration, transport, and collection from the active layer of the cell.

The current-voltage (I-V) characteristics and MPC measurements are performed under constant bias V_b. Figure 1 displays the I-V characteristics of a BHJ rrP3HT/PCBM OPV cell photoexcited by the Sun spectrum and intensity. The measured open-circuit voltage is $V_{OC} = 0.73$ V, short-circuit current $I_{SC} = 11.4$ mA/cm^2, and the extracted fill factor and PCE are FF $= 0.52$ and PCE $= 4.4\%$, respectively.

For the MPC measurements, the OPV devices are transferred to a low-temperature cryostat that is placed in a magnetic field B. The magnetic field is provided by a

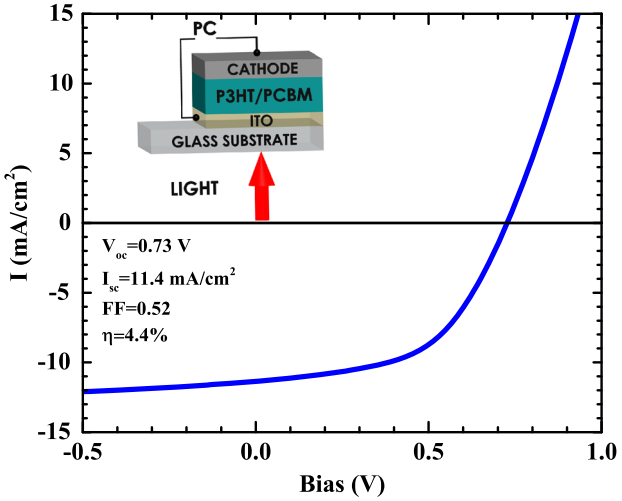

FIG. 1. I-V characteristics response of BHJ rrP3HT/PCBM photovoltaic cell with PCE $= 4.4\%$ under Sun illumination (blue line) at $B = 0$. The magnetophotocurrent studied represents the variations of the short-circuit current with magnetic field. The inset shows the structure of the cell.

superconducting magnet with B up to approximately 8.5 T. The measured device is immersed in helium vapors, and the temperature is controlled by the helium flow and a heater. The OPV devices are illuminated with a 405-nm laser diode (Sanyo) of nominal power of 40 mW. The light from the laser diode is directed through a set of lenses and neutral density filters onto the sample at the bottom of the cryostat of the superconducting magnet (approximately 1 m away from the laser diode). The actual impinged light intensity on the device is approximately 1 mW/mm^2 (approximately one sun) at room temperature; below approximately 100 K, we increase the excitation intensity by a factor of approximately 2 since the photocurrent is too small. The photocurrent is measured at zero bias ($V_b = 0$) while sweeping the external magnetic field. Some of the measurements are done using a 470-nm light-emitting diode; no apparent changes in the measured MPC(B) are detected. Care is taken to electrically connect the device using twisted nonmagnetic wires made of phosphor bronze alloy; the resistance ratio of the wire to the device is typically 10^{-7}; thus, the effect of its magnetoresistance (approximately $-3 \times 10^{-3}\%$) [24] on the total MPC is negligibly small. Also, the static magnetic field produced by the small current in the twisted wires and the device itself is negligibly small ($\ll 10^{-4}$ T). MPC is defined as MPC(B) $=$ [PC(B)/PC(0) $-$ 1], where PC is the measured short-circuit current under illumination. The data presented in the figures below are the result of averaging many magnetic field sweeps but otherwise are not smoothed.

III. EXPERIMENTAL RESULTS

Figures 2(a) and 2(b) show the magnetic field response of the short-circuit current MPC(B) up to $B \sim 8$ T for various temperatures in the range of $T = 10$–320 K. Enlarged view of the very-low-field region is shown in Figs. 2(c) and 2(d). The sharp feature [full width at half maximum (FWHM) of approximately 10 mT] observed in Figs. 2(c) and 2(d) is the typical MPC(B) response due to spin mixing by the proton-polaron HF interaction, which for P3HT is of the order of $a_{HF} \sim 0.5$ μeV (HF field, $B_{HF} \sim 4$ mT) [8]. At higher fields, the response due to the HF interaction saturates so that other spin-mixing interactions that are operative at high fields become dominant. The HF contribution to magnetoconductance (MC) in organic devices has been accounted for in detail in various studies [2,8,11]; here, we concentrate on the high-field region shown in Figs. 2(a) and 2(b) in two temperature ranges, namely, high T (100–320 K) and low T (10–100 K), respectively. It is clearly seen that the MPC(B) response does not saturate even at the highest field studied here. In the high-temperature region [Fig. 2(a)], MPC(B) increases with B (for $B > \sim 1$ T), whereas in the low-temperature region [Fig. 2(b)], it decreases with B, indicating that two different spin-mixing mechanisms are involved. In our previous report [17], we attribute the high-field behavior

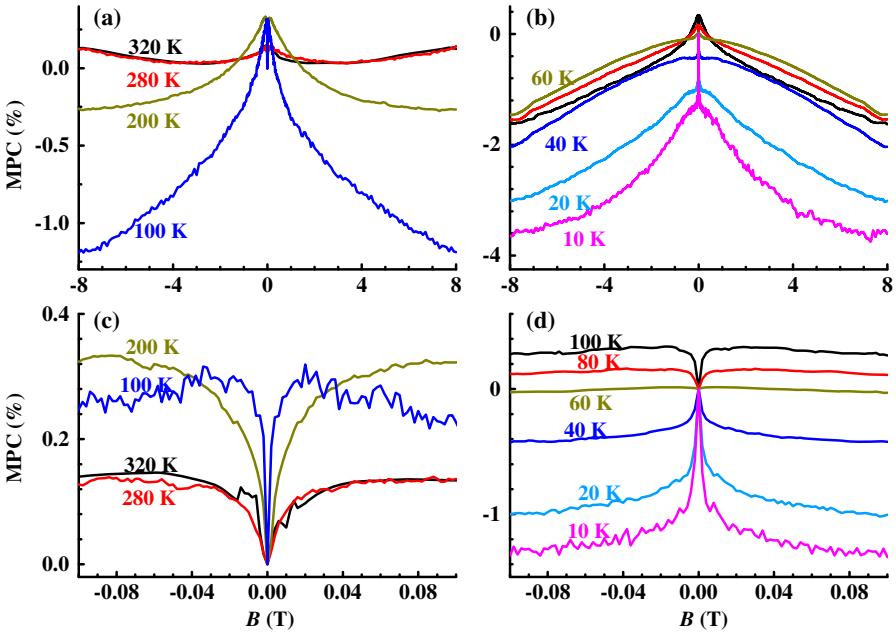

FIG. 2. MPC(B) response of rrP3HT/PCBM photovoltaic cell at various temperatures at $V = 0$. (a) $T = 320$, 280, 200, 100 K at $|B|$ up to 8 T. Same color code as in (c). (b) $T = 100$, 80, 60, 40, 20, 10 K at $|B|$ up to 8 T. Same color code as in (d). (c) Same as (a) on an enlarged scale, $|B| < 0.1$ T. Same color code as in (a). (d) Same as (b) on an enlarged scale, $|B| < 0.1$ T. Same color code as in (b).

at high temperatures to the Δg mechanism operating within the short-lived CTE. In the low-temperature region, we now include the effect of thermal spin polarization (TSP) that was found [19] to affect both MC in illuminated organic devices under forward bias voltage and magnetoelectroluminescence (MEL) at low temperatures and high fields.

IV. HIGH-FIELD MODELS

The main processes discussed in this paper occur after the photoexcited SE ionizes to promote photocurrent; the SE is spinless, and, thus, a magnetic field cannot directly influence its population. Thus, the obtained MPC is the result of intermediate processes in which transient photogenerated pairs of spin $S = ½$ charges (spin pair, SP) are not fully separated and may exist in either overall spin-triplet ($S = 1$) or spin-singlet ($S = 0$) configurations. Any mechanism within the SP that renders the photocurrent to be magnetic field sensitive ought to include a dissociation (and/or recombination) process which is spin dependent; namely, there exists "symmetry breaking" between SP of the overall spin singlet (SP_S) and triplet (SP_T). In many cases, a slight symmetry breaking in the SP_S and SP_T dissociation or recombination rates of only approximately 1%–5% is sufficient to cause MPC of the order of a few percent [8,11,25]. We note that spin-dependent recombination rates have indeed been found in recent dielectric polarizability experiments [21] in P3HT/PCBM blends.

Given the existence of asymmetry between SP_S and SP_T, we now consider two mechanisms that may be effective at high fields: (a) The Δg mechanism and (b) spin polarization in thermal equilibrium caused by the high-field Zeeman splitting. The former mechanism was discussed in some detail in previous reports [17,26]; here, we summarize it for completeness.

A. The Δg mechanism

For spin pairs (e.g., radical pairs, PPs, or CTEs) that are composed of two spin-½ species with different g factors, a known spin-mixing mechanism that is more efficient at higher fields is the so-called Δg mechanism, where Δg is the difference in the g factor of the two spin-½ particles [14,18,27,28]. The nonidentical precession frequencies of the two individual spins at finite B causes SP_S to transform into the T_0 state of SP_T and vice versa [29] at a rate $\Delta\omega_p = \mu_B \Delta g B/h$, which increases with B leading to a more effective spin mixing at higher fields.

In order to account for the Δg mechanism quantitatively while keeping the discussion simple, we disregard the HF interaction and consider only the Zeeman and exchange-interaction terms in the spin Hamiltonian. Since the HF field is of the order of approximately 3 mT, then neglecting the HF interaction is justified for MPC(B) response at fields much higher than the HF field. In the solid state, the diffusion of spin pairs is small, and with the low density of carriers, we may disregard diffusion and reencounter of carriers after the spin pair has decayed; these effects are important in biochemical reactions in solution [27]. Consequently, the SP Hamiltonian in a magnetic field B is $H = \sum_i g_i \mu_B \vec{B} \cdot \vec{S}_i - J(\vec{S}_1 \cdot \vec{S}_2 + 1/4)$, where J is the exchange interaction coefficient, and g_i ($g_1 \neq g_2$) is the g factor of spin $S_i = ½$. The exchange interaction in PPs or CTEs is small, of the order of $J/2\mu_B < 10$ mT; thus, any anisotropy in J will not show up at high fields. The g factor of localized polarons in P3HT is anisotropic, but the anisotropy is smaller than the difference $\Delta g = g_2 - g_1$ between P3HT and PCBM. Thus, for the high field, spin mixing is sufficient [30] to take into account the effect of Δg only. At $B = 0$, the four eigenstates may be divided

into a singlet (ψ_S) and threefold degenerate triplet states (ψ_{T+}, ψ_{T0}, ψ_{T-}). For $B \neq 0$, the states are Zeeman separated into four levels:

$$\begin{aligned} &E_{1,4} = [-J \mp (g_1 + g_2)\mu_B B/2]/2; \qquad \psi_{1,4} = \psi_{T\mp}, \\ &E_{2,3} = \mp J/(2\cos\theta); \\ &\psi_{2,3} = \cos(\theta/2)\psi_{T0,S} \mp \sin(\theta/2)\psi_{S,T0}, \end{aligned} \tag{1}$$

where $\tan\theta = \hbar\Delta\omega_p/J$. Equation (1) shows that only the singlet- (S) and T_0 triplet-spin wave functions mix, thereby, the spin character of each mixed state [labeled 2 and 3 in Eq. (1)] becomes B dependent. Consequently, at finite fields the S and T_0 states are not eigenstates of the system causing the initial photoexcited S-state population to oscillate between levels 2 and 3 [Eq. (1)] with frequency $|E_2 - E_3|/h \sim 2\Delta\omega_p$ at high fields. These oscillations can be described by using the time-dependent density matrix, $\sigma(t) = e^{-iHt/\hbar}\sigma_0 e^{iHt/\hbar}$ with $\sigma_0 = \sigma(t = 0)$. The singlet and T_0 densities are then given by $\rho_{S,T_0}(t) = \mathrm{Tr}[P^{S,T0}\sigma(t)] = (1 \pm \cos^2\theta)/2 \pm (sin^2\theta\cos\omega_{23}t)/4$, where, $P^{S,T0}$ is the projection operator, Tr denotes the trace, and $\omega_{23} = (E_2 - E_3)/h$. It is, thus, seen that the system oscillates between singlet and T_0 states at a frequency that is determined by Δg. It is then clear that the total SP number density $\rho(t) = \rho_S(t) + \rho_{T0}(t)$ is conserved and is field independent. No decay was assumed for the calculated S, T_0 densities above, but any real system is dissipative. Eventually, the SP either dissociates into free charges that contribute to the PC or recombine. We denote the spin-dependent decay rates by κ_S and κ_T for the SP in the singlet and triplet configurations, respectively. The decay rate κ measures the rate at which spin pairs disappear both by dissociation to free carriers (that contribute to the photocurrent) and by recombination. The effective decay rate associated with the SP levels $n = 1, ..., 4$ is then given by [31,32]

$$\gamma_n = \sum_{\lambda=S,T} \kappa_\lambda P^\lambda_{nn}, \tag{2}$$

where P^λ_{nn} is the nth diagonal matrix elements of the projection operator for $\lambda = S$ or T configurations; note that since S-T_0 mixing is B dependent so is P^λ_{nn}. When the decay is included, then the SP density also decays taking the form [31,32] $\rho_\lambda(t) = \sum_{mn} P^\lambda_{mn}(\sigma_0)_{nm}\exp(i\omega_{nm}t - \gamma_{nm}t)$, where $\lambda = S, T_0$, $\omega_{nm} = (E_n - E_m)/h$, and $\gamma_{nm} = \gamma_n + \gamma_m$. Note that $\omega_{23} = J/(h\cos\theta)$, $\gamma_2 = \kappa_S\cos^2(\theta/2) + \kappa_{T0}\sin^2(\theta/2)$, and $\gamma_3 = \kappa_S\sin^2(\theta/2) + \kappa_{T0}\cos^2(\theta/2)$ are all field dependent.

The SP dissociation contributes to the photocurrent. The S and T dissociation rates k_{DS} and k_{DT} may be spin dependent. The steady-state photocurrent is then given by

$$\begin{aligned} \mathrm{PC}_{\Delta g}(B) &\propto \sum_{\lambda=S,T_0} k_{D\lambda}\int_0^\infty \rho_\lambda(t)dt \\ &= \frac{(k_{\mathrm{DS}} - k_{\mathrm{DT}})2\tau_{23}c^2s^2}{1 + (\omega_{23}\tau_{23})^2} + \tau_{22}c^2(c^2k_{\mathrm{DS}} + s^2k_{\mathrm{DT}}) \\ &\quad + \tau_{33}s^2(s^2k_{\mathrm{DS}} + c^2k_{\mathrm{DT}}), \end{aligned} \tag{3}$$

where for photoexcited SP, we take $\sigma_0 = P^S$. In Eq. (3), $\tau_{nm} = 1/\gamma_{nm}$, and $c = \cos(\theta/2)$, $s = \sin(\theta/2)$. $\mathrm{PC}_{\Delta g}(B)$ is the SP contribution to the photocurrent through the Δg mechanism. The contribution of the Δg mechanism to MPC is then obtained from Eq. (3) using the definition $\mathrm{MPC}_{\Delta g}(B) = \mathrm{PC}_{\Delta g}(B)/\mathrm{PC}_{\Delta g}(0) - 1$. It is easily verified that for spin-independent decay, $\kappa_S = \kappa_T$ and $k_{\mathrm{DS}} = k_{\mathrm{DT}}$, the SP density ($=k_D/2\kappa$) is field independent and $\mathrm{MPC}_{\Delta g} \equiv 0$. Equation (3) shows that for short decay times, $\omega_{23}\tau_{23} < 1$ and $\Delta g\mu_B B \gg J$, the profile of the calculated $\mathrm{MPC}_{\Delta g}(B)$ is nearly Lorentzian with FWHM approximately $\hbar/(\Delta g\mu_B\tau)$, where $\tau = \tau_{23} = 1/(\kappa_S + \kappa_{T0})$.

The Lorentzian line shape predicted by Eq. (3) is the result of the assumed exponential decay process. In disordered materials such as those used in the present study, the decay process is found in many cases to be nonexponential, i.e., much slower [33,34]. Experimental data in amorphous materials have been widely interpreted in terms of the Kohlrausch-Williams-Watts (KWW) function, the so-called "stretched-exponential" decay [33,34], $\exp(-t/\tau_K)^\beta$ with $\beta < 1$, or by a sublinear power-law decay caused by multiple trapping [35]. This nonexponential decay is equivalent to having a broad distribution of decay times [36]. Using this approach, the time-dependent free-carrier-density profile should now be described by a dispersive decay rather than by an exponential decay; this leads to a "dispersive" B dependence rather than a Lorentzian $\mathrm{MPC}_{\Delta g}(B)$ response. A simple dispersive function that has been widely used to replace the Lorentzian function in Eq. (3) is the Cole-Cole function [36–38], $[1 + (\omega_{23}\tau_{23})^2]^{-1} \to \mathrm{Re}[1 + (i\omega_{23}\tau_{23})^\alpha]^{-1}$, where Re denotes the real part, and $\alpha \leq 1$ is the dispersive parameter; α can be related numerically to the KWW stretched exponent β [36]. Similarly, the frequency-domain dispersive parameter α can be related to the sublinear time-domain power-law exponent [35]. The implementation of the Cole-Cole function has been proven useful in a variety of experiments such as dielectric spectroscopy [36] and photomodulation measurements [38–42], where the frequency dependence of the measured quantities can be explained with a decay time distribution.

B. The thermal spin-polarization model

The contribution of TSP in high magnetic fields (so-called "spin statistics") was recently considered by Wang *et al.* [19] for explaining the low-temperature MEL(B) response in organic light-emitting diodes and MC(B) response in bias-driven organic photovoltaic cells. For

the effect of TSP on the measured MPC (at zero bias), we consider SP species in complete thermal equilibrium. Under these conditions, the fraction of pairs in each of the four spin sublevels E_n [$n = 1, \ldots, 4$, Eq. (1)] is

$$\rho_n^{\mathrm{th}} = e^{-b_n} / \sum_j e^{-b_j}, \tag{4}$$

where $b_n = E_n/k_BT$ is the level "polarizing parameter," and k_B is the Boltzmann constant. Starting at $t = 0$ from any given configuration ρ_n^0, the system evolves toward thermal equilibrium in an exponential process with a time constant dominated by the material spin-relaxation time τ_S; therefore, the thermal equilibrium fractions [Eq. (4)] are reached after a time $t \gg \tau_S$. Consequently, for $B = 0$ and $J \ll k_BT$ Eqs. (4) and (1) lead to a nearly uniform thermal distribution,$\rho_n^{\mathrm{th}} \approx 1/4$, whereas for large B and/or small T, the lowest level is predominantly populated with a distribution: $\rho_1^{\mathrm{th}} \gg \rho_{2,3}^{\mathrm{th}} \gg \rho_4^{\mathrm{th}}$. Neglecting any spin-mixing mechanism that may occur prior to thermal equilibrium but taking into account the pairs' decay process, the time-dependent-level occupation density may be calculated using the following set of rate equations:

$$d\rho_n(t)/dt = -\gamma_n\rho_n - \left[\rho_n - \left(\sum_j \rho_j\right)\rho_n^{\mathrm{th}}\right]/\tau_S \quad (n = 1, \ldots, 4). \tag{5}$$

In Eq. (5), the first term on the rhs describes the spin-dependent decay [the level decay rate γ_n is given by Eq. (2) above], whereas the second term in the rhs describes the evolution toward thermal equilibrium. Consequently, the spin sublevel populations become magnetic field and time dependent. Solving Eqs. (5) with the proper initial conditions (e.g., only the S configuration is initially photogenerated), we obtain the solutions $\rho_n(t, B)$. Consequently, the contribution of TSP to the photocurrent $\mathrm{PC_{th}}$ at steady state ($t \to \infty$) is proportional to the total dissociation yield:

$$\mathrm{PC_{th}}(B) \propto \sum_n k_{Dn} \int_0^\infty \rho_n(t, B)dt, \tag{6}$$

where $k_{Dn} = \sum_{\lambda=S,T} k_{D\lambda} P_{nn}^{\lambda}$ is the level dissociation rate. For $B = 0$, we have $k_{D1,2,4} = k_{\mathrm{DT}}$, $k_{D3} = k_{\mathrm{DS}}$, whereas for high fields $k_{D1,4} = k_{\mathrm{DT}}$ and $k_{D2,3} = (k_{\mathrm{DS}} + k_{\mathrm{DT}})/2$. The contribution of TSP to the magnetophotocurrent $\mathrm{MPC_{th}}$ is then obtained from Eq. (6): $\mathrm{MPC_{th}}(B) = \mathrm{PC_{th}}(B)/\mathrm{PC_{th}}(0) - 1$. The calculated $\mathrm{MPC_{th}}$ is the contribution of thermal polarization to MPC in the absence of any spin-mixing mechanism. The total MPC is, thus, the weighted sum of $\mathrm{MPC_{th}}$ and the contribution of the spin-mixing processes [e.g., the Δg mechanism, Eq. (3)].

V. DISCUSSION

We now analyze the high-field response using the models discussed above, namely, the Δg and TSP mechanisms. Equation (3) for the Δg mechanism is obtained under the assumption that the time it takes for the spin mixing by this mechanism is much shorter than the SP decay time τ, and the spin lattice relaxation time τ_S, which is the time constant to reach thermal equilibrium. On the other hand, Eq. (6) for the steady-state thermal polarization contribution explicitly takes into account the system decay (i.e., dissociation and recombination). We, therefore, use as an approximation for the MPC response a weighted sum of MPC components as follows:

$$\mathrm{MPC}(B) = \mathrm{MPC}_{\Delta g} + \mathrm{MPC_{th}} + \mathrm{MPC_{HF}}. \tag{7}$$

In Eq. (7), we add a HF Lorentzian response term to account for the very low field having the response $\mathrm{MPC_{HF}} = W_{\mathrm{HF}}B^2/(B^2 + {B_{\mathrm{HF}}}^2)$, where W_{HF} is the weight and $B_{\mathrm{HF}} \sim 4$ mT. We emphasize that $\mathrm{MPC_{HF}}$ varies with B only at very low fields; for $B \gg B_{\mathrm{HF}}$, the HF contribution is field independent. We choose to separate the HF contribution in Eq. (7) since at low fields, MPC due to the HF interaction originates also from long-lived PPs (e.g., hole on P3HT and electron not on PCBM or not localized polarons) that do not contribute to the Δg mechanism. The various HF contributions (which may be either positive or negative) add up algebraically to the weight W_{HF} in Eq. (7). In any case, their effect is negligibly small at high fields.

In order to extract the relative contributions of the TSP and Δg MPC components, we fit the experimental data (Fig. 2) using Eq. (7) taking into account the following. We use a fixed $\Delta g = 0.002$ for the P3HT/PCBM system [17]. The main parameter that determines the relative weight of the TSP and Δg mechanisms is the ratio τ/τ_S, where $\tau^{-1} = (\kappa_S + \kappa_T)$; see Eq. (5). The SL relaxation times τ_S of excess charges in light-induced P3HT/PCBM blends are measured for various photoexcitation wavelengths in the temperature range 77–200 K [43]. For annealed samples, τ_S varies from approximately 1 μs $\pm$ 50% at 77 K to approximately 0.3 μs $\pm$ 30% at 200 K. We assume that outside of this temperature range there are no significant changes in τ_S. Since the fitting parameter τ/τ_S changes by a factor of approximately 5×10^3 (see Table I) in our measured temperature range, a factor of approximately 2 or so in τ_S should not significantly change the fitting results. From these data, we can estimate τ^{-1}, which is used to calculate $\mathrm{MPC}_{\Delta g}$. We assume a uniform decay rate for all triplet configurations ($T_{\pm,0}$) and use the dissociation rate ratio $k_{\mathrm{DS}}/k_{\mathrm{DT}}$ as one of the temperature-dependent fitting parameters. For the HF interaction field, we use $B_{\mathrm{HF}} =$ 4.3 mT [8,11] and adjust the strength and sign of W_{HF} to reproduce MPC at very low field at each temperature. We note that the HF is influenced by contributions from various sources [17]; thus, we do not attempt to fit it within the high-field models discussed here. We have also allowed for a modest exchange interaction for CTEs [44] ($J/g\mu_B \sim 1$–5 mT) and a dispersive recombination parameter

TABLE I. Best-fitting parameters for the MPC(B) response for the temperature range 10–290 K. Second row: τ/τ_S is the ratio of the SP decay time to the spin lattice relaxation time. Third row: The measured spin lattice relaxation time taken from Ref. [43] for the annealed samples. The variations in the measured values are ±50% at 77 K decreasing gradually to ±30% at 200 K. The values in parentheses are extrapolation for lower and higher temperatures (we conjecture no more than a factor of approximately 2 error bar on these extrapolated values). Fourth row: k_{DT0}/k_{DS}, the ratio of the SP triplet T_0 to singlet dissociation rates. For $k_{DT0}/k_{DS} < 1$ (>1) $MPC_{\Delta g}$ and MPC_{th} have the same (opposite) signs (see text). Fifth row: Δg:TSP_{8T}, the weight ratio of the Δg-to-TSP components at $B = 8$ T; the negative sign above 250 K signifies opposite signs of the two mechanisms. Sixth row: α, the dispersive parameter in the $MPC_{\Delta g}(B)$ response component (see text). Because of the low sensitivity of the response profile to α, we estimate ±0.1 error bar in the extracted values.

T (K)	10	20	40	60	80	100	160	200	250	290
τ/τ_S	3.8	10	1.1	0.1	3×10^{-3}	1.2×10^{-3}	2.2×10^{-3}	2.5×10^{-3}	6.2×10^{-4}	7.7×10^{-4}
τ_S (μs) [43]	(1)	(1)	(1)	(1)	1.3	1.5	0.5	0.25	(0.2)	(0.2)
k_{DT0}/k_{DS}	0.99	0.7	0.93	0.94	0.99	0.95	0.99	0.98	1.45	1.2
Δg:TSP_{8T}	0.7	0.5	0.7	0.7	0.4	0.4	0.3	0.3	−1.2	−1.8
α	0.6	0.7	0.6	0.6	0.9–1	0.9–1	0.9–1	0.9–1	0.9–1	0.9–1

($\alpha \sim 0.5$–1), although the data are less sensitive to variations in these parameters. The magnitude of the exchange interaction is reasonable for CTEs in P3HT/PCBM blends, and it does not affect the response at high fields. For the amorphous blends used in our devices, it is not surprising that a temperature-dependent decay time and, consequently, a dispersive parameter $\alpha \leq 1$ is obtained. Above $T = 80$ K, where τ/τ_S becomes much smaller than 1, the response is less sensitive to variations in α, and the data can be fit with nearly nondispersive recombination, $\alpha \cong 0.9$–1. The results of the fits are shown in Fig. 3 at several representative temperatures (similar quality fits are obtained at all other temperatures). Table I summarizes the best-fitting parameters. It is seen that $MPC_{\Delta g}$ is positive at high temperatures and reverses its sign below approximately 250 K; in parallel, the fitting parameter $k_{DS}/k_{DT} > 1$ at high temperatures and is smaller than 1 at low temperatures. Note that MPC_{th} is negative at all temperatures and does not change sign. The different behavior of $MPC_{\Delta g}$ and MPC_{th} stems from the fact that in the Δg mechanism only the S and T_0 levels are involved, whereas in the TSP mechanism, the dissociation from all four levels determines the PC. Therefore, a much larger change in k_{DS}/k_{DT} is needed in order to reverse the sign of MPC_{th}.

Figure 4 shows an Arrhenius plot of the extracted average decay rate as a function of temperature. It is seen that the decay rate decreases sharply with decreasing temperature from approximately 3×10^9 s^{-1} at room

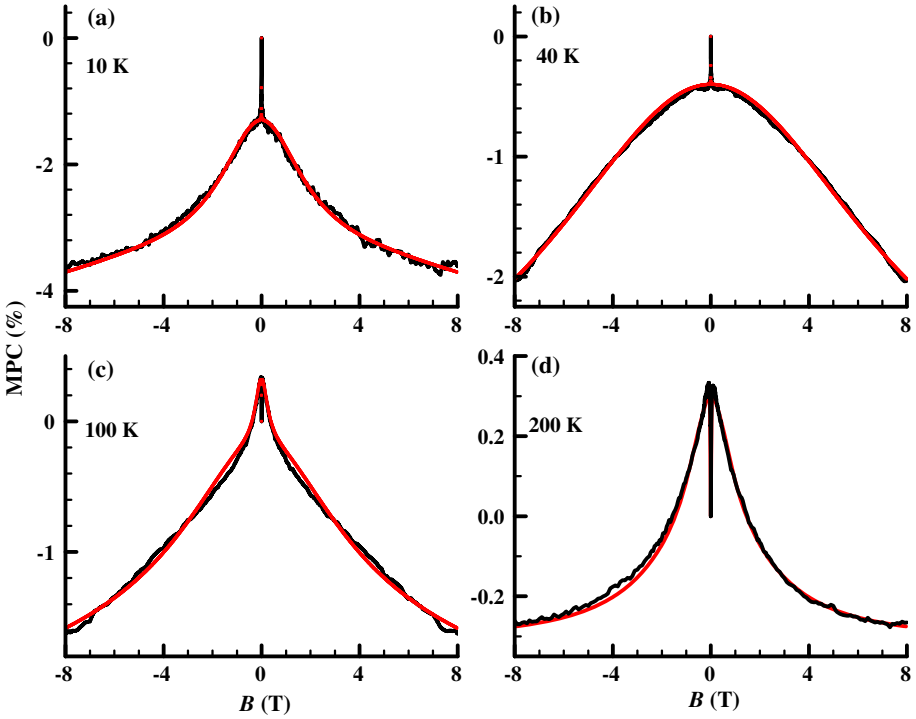

FIG. 3. Representative fits of the MPC(B) response shown in Fig. 2 using the Δg-TSP model [Eq. (7)]. Black lines, experimental data; red dots, fits obtained using Eq. (7). Note that the fits contain the HF interaction ($B < 0.01$ T); this is barely visible in the expanded scale of the figure.

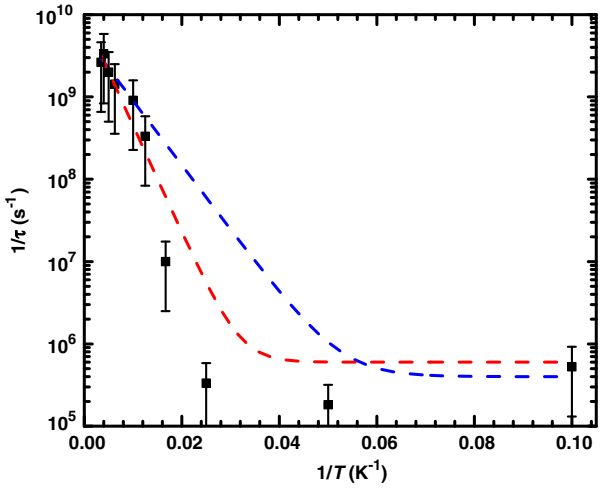

FIG. 4. Arrhenius plot of the extracted SP decay rate obtained from the MPC(B) fits (Table I and Fig. 3). The estimated error in the decay rate is about a factor of 2. The dashed lines represent two possible fits with activation energies in the range $E_a/k_B =$ 180 K (blue dashed line) and $E_a/k_B = 300$ K (red dashed line).

temperature to a constant value τ_L^{-1}, where $\tau_L^{-1} \sim 5 \times 10^5$ s^{-1} for $T < 40$ K (see, also, Table I). The dashed lines represent fits to a thermally activated behavior $\tau^{-1} = \nu \exp(-E_a/k_BT) + \tau_L^{-1}$ with activation energies as marked. We, thus, conclude that there exists a distribution of activation energies in the range 0.015–0.026 eV. Although there appear to be large variations in the derived values of τ^{-1} vs temperature, it is, nevertheless, clear that τ^{-1} decreases (in a thermally activated fashion) by approximately 4 orders of magnitude as the temperature decreases from 300 to approximately 40 K. The very short decay time obtained at room temperature ($\tau \sim 0.3$ ns) corresponds to previous measurements of the decay time of CTEs at $B = 0$ [17,45]. It, thus, appears that the short decay time inhibits larger values of the MPC. An OPV cell with longer CTE decay at room temperature will show higher MPC values, which may be more easily utilized.

VI. CONCLUSIONS

We show that both the Δg mechanism and thermal spin polarization contribute to the magnetophotoconductance response at high fields and low temperatures in organic photovoltaic devices. The key parameter that determines the relative contribution of each mechanism is the ratio of the spin-pair lifetime to the spin lattice relaxation time, τ/τ_S. In rrP3HT/PCBM blends, while τ_S increases by only a factor of approximately 5 as the temperature decreases from 300 to 40 K, τ increases by approximately 4 orders of magnitude, rendering the TSP mechanism to dominate the MPC response at low temperatures. The opposite contribution of the two MPC mechanisms and their characteristic lifetime explain the polarity change of the high-field MPC(B) response in the rrP3MT/PCBM blend at low temperatures.

The present study shows that by using organic donor-acceptor blends having relatively large difference in the D and Ag factors and long electron-hole recombination times, then the magnetic field effect on the photocurrent, and, in turn, also on PCE may reach substantial values (>50%) even at room temperature. Such an effect may pave the way to magnetodevices operated by sunlight illumination.

ACKNOWLEDGMENTS

This work is supported in part by the U.S.-Israel Binational Science Foundation (Grant No. 2010135, Z. V. V., N. T., and E. E.), and the National Science Foundation Materials Research Science and Engineering Center (MRSEC) at the University of Utah (Grant No. DMR11-21252), Z. V. V.).

[1] O. Mermer, G. Veeraraghavan, T. L. Francis, Y. Sheng, D. T. Nguyen, M. Wohlgenannt, A. Kohler, M. K. Al-Suti, and M. S. Khan, Large magnetoresistance in nonmagnetic π-conjugated semiconductor thin film devices, Phys. Rev. B **72**, 205202 (2005).

[2] V. Prigodin, J. Bergeson, D. Lincoln, and A. J. Epstein, Anomalous room temperature magnetoresistance in organic semiconductors, Synth. Met. **156**, 757 (2006).

[3] P. Desai, P. Shakya, T. Kreouzis, W. P. Gillin, N. A. Morley, and M. R. J. Gibbs, Magnetoresistance and efficiency measurements of Alq_3-based OLEDs, Phys. Rev. B **75**, 094423 (2007).

[4] B. Hu and Y. Wu, Tuning magnetoresistance between positive and negative values in organic semiconductors, Nat. Mater. **6**, 985 (2007).

[5] J. D. Bergeson, V. N. Prigodin, D. M. Lincoln, and A. J. Epstein, Inversion of Magnetoresistance in Organic Semiconductors, Phys. Rev. Lett. **100**, 067201 (2008).

[6] P. Shakya, P. Desai, T. Kreouzis, W. P. Gillin, S. M. Tuladhar, A. M. Ballantyne, and J. Nelson, The effect of applied magnetic field on photocurrent generation in poly-3-hexylthiophene:-phenyl C61-butyric acid methyl ester photovoltaic devices, J. Phys. Condens. Matter **20**, 452203 (2008).

[7] H. Zang, Z. Xu, and B. Hu, Magneto-optical investigations on the formation and dissociation of intermolecular charge-transfer complexes at donor-acceptor interfaces in bulk-heterojunction organic solar cells, J. Phys. Chem. B **114**, 5704 (2010).

[8] T. D. Nguyen, G. Hukic-Markosian, F. J. Wang, L. Wojcik, X. G. Li, E. Ehrenfreund, and Z. V. Vardeny, Isotope effect in spin response of π-conjugated polymer films and devices, Nat. Mater. **9**, 345 (2010).

[9] J. Kalinowski, M. Cocchi, D. Virgili, P. Di Marco, and V. Fattori, Magnetic field effects on emission and current in Alq3-based electroluminescent diodes, Chem. Phys. Lett. **380**, 710 (2003).

[10] P. A. Bobbert, T. D. Nguyen, F. W. A. van-Oost, B. Koopmans, and M. Wohlgenannt, Bipolaron Mechanism

for Organic Magnetoresistance, Phys. Rev. Lett. **99**, 216801 (2007).
[11] T. D. Nguyen, B. R. Gautam, E. Ehrenfreund, and Z. V. Vardeny, Magnetoconductance Response in Unipolar and Bipolar Organic Diodes at Ultrasmall Fields, Phys. Rev. Lett. **105**, 166804 (2010).
[12] T. D. Nguyen, G. Hukic-Markosian, F. Wang, X.-G. Li, E. Ehrenfreund, and Z. V. Vardeny, The hyperfine interaction role in the spin response of π-conjugated polymer films and spin valve devices, Synth. Met. **161**, 598 (2011).
[13] P. A. Bobbert, W. Wagemans, F. W. A. van Oost, B. Koopmans, and M. Wohlgenannt, Theory for Spin Diffusion in Disordered Organic Semiconductors, Phys. Rev. Lett. **102**, 156604 (2009).
[14] H. Hayashi, *Introduction to Dynamic Spin Chemistry; Magnetic Field Effects on Chemical and Biochemical Reactions* (World Scientific Publishing Co., Singapore, 2004).
[15] A. J. Schellekens, W. Wagemans, S. P. Kersten, P. A. Bobbert, and B. Koopmans, Microscopic modeling of magnetic-field effects on charge transport in organic semiconductors, Phys. Rev. B **84**, 075204 (2011).
[16] B. R. Gautam, T. D. Nguyen, E. Ehrenfreund, and Z. V. Vardeny, Magnetic field effect on excited-state spectroscopies of π-conjugated polymer films Phys. Rev. B **85**, 205207 (2012).
[17] A. H. Devir-Wolfman, B. Khachatryan, B. R. Gautam, L. Tzabary, A. Keren, N. Tessler, Z. V. Vardeny, and E. Ehrenfreund, Short lived charge transfer excitons in organic photovoltaic cells studied by high field magnetophotocurrent, Nat. Commun. **5**, 4529 (2014).
[18] R. H. Friend, M. Phillips, A. Rao, M. W. B. Wilson, and C. R. McNeill, Excitons and charges at organic semiconductor heterojunctions, Faraday Discuss. **155**, 339 (2012).
[19] J. Wang, A. Chepelianskii, F. Gao, and N. C. Greenham, Control of exciton spin statistics through spin polarization in organic optoelectronic devices, Nat. Commun. **3**, 1191 (2012).
[20] S. Gélinas, A. Rao, A. Kumar, S. L. Smith, A. W. Chin, J. Clark, T. S. v. d. Poll, G. C. Bazan, and R. H. Friend, Ultrafast long-range charge separation in organic semiconductor photovoltaic diodes, Science **343**, 512 (2014).
[21] S. L. Bayliss, N. C. Greenham, R. H. Friend, H. Bouchiat, and A. D. Chepelianskii, Spin dependent recombination probed through the dielectric polarizability, Nat. Commun. **6**, 8534 (2015).
[22] A. Rao, M. W.B. Wilson, J. M. Hodgkiss, S. Albert-Seifried, H. Bassler, and R. H. Friend, Exciton fission and charge generation via triplet excitons in pentacene/C60 bilayers, J. Am. Chem. Soc. **132**, 12698 (2010).
[23] Y. Zhang, T. P. Basel, X. Yang, D. J. Mascaro, F. Liu, and Z. V. Vardeny, Spin-enhanced organic bulk heterojunction photovoltaic solar cells, Nat. Commun. **3**, 1043 (2012).
[24] M. Abrecht, A. Adare, and J. W. Ekin, Magnetization and magnetoresistance of common alloy wires used in cryogenic instrumentation, Rev. Sci. Instrum. **78**, 046104 (2007).
[25] T. D. Nguyen, T. P. Basel, Y.-J. Pu, X.-G. Li, E. Ehrenfreund, and Z. V. Vardeny, Isotope effect in the spin response of aluminum tris(8-hydroxyquinoline) based devices Phys. Rev. B **85**, 245437 (2012).
[26] B. Khachatryan, A. H. Devir-Wolfman, L. Tzabary, A. Keren, N. Tessler, Z. V. Vardeny, and E. Ehrenfreund, High field magneto-photocurrent in organic bulk hetero-junction photo-voltaic cells, Synth. Met. **208**, 49 (2015).
[27] Y. Tanimoto, H. Hayashi, S. Nagakura, H. Sakuragi, and K. Tokumaru, The external magnetic field effect on the singlet sensitized photolysis of dibenzoyl peroxide, Chem. Phys. Lett. **41**, 267 (1976).
[28] K. Schulten and I. R. Epstein, Recombination of radical pairs in high magnetic fields: A path integral–Monte Carlo treatment, J. Chem. Phys. **71**, 309 (1979).
[29] N. J. Turro, Influence of nuclear spin on chemical reactions: Magnetic isotope and magnetic field effects, Proc. Natl. Acad. Sci. U.S.A. **80**, 609 (1983).
[30] B. Khachatryan and E. Ehrenfreund (unpublished).
[31] E. Ehrenfreund and Z. V. Vardeny, Effects of magnetic field on conductance and electroluminescence in organic devices, Isr. J. Chem. **52**, 552 (2012).
[32] C. R. Timmel, U. Till, B. Brocklehurst, K. A. McLauchlan, and P. J. Hore, Effects of weak magnetic fields on free radical recombination reactions, Mol. Phys. **95**, 71 (1998).
[33] G. Pfister and H. Scher, Dispersive transient transport in disordered solids, Adv. Phys. **27**, 747 (1978).
[34] F. Alvarez, A. Algeria, and J. Colmenero, Relationship between the time-domain Kohlrausch-Williams-Watts and frequency-domain Havriliak-Negami relaxation function, Phys. Rev. B **44**, 7306 (1991).
[35] M. Westerling, R. Osterbacka, and H. Stubb, Recombination of long-lived photoexcitations in regioregular polyalkylthiophenes, Phys. Rev. B **66**, 165220 (2002).
[36] A. Bello, E. Laredo, and M. Grimau, Distribution of relaxation times from dielectric spectroscopy using Monte Carlo simulated annealing: Application to PVDF, Phys. Rev. B **60**, 12764 (1999).
[37] K. S. Cole and R. H. Cole, Dispersion and absorption in dielectrics, J. Chem. Phys. **9**, 341 (1941).
[38] O. Epshtein, G. Nakhmanovich, Y. Eichen, and E. Ehrenfreund, Dispersive dynamics of photoexcitations in conjugated polymers measured by photomodulation spectroscopy, Phys. Rev. B **63**, 125206 (2001).
[39] O. Epshtein, Y. Eichen, E. Ehrenfreund, M. Wohlgenannt, and Z. V. Vardeny, Linear and Nonlinear Photoexcitation Dynamics in Conjugated Polymers, Phys. Rev. Lett. **90**, 046804 (2003).
[40] E. Gershman, T. Drori, C. Herzog, Y. Eichen, and E. Ehrenfreund, Recombination kinetics of photoexcitations in films of MEH-PPV and MEH-PPV/C_{60} mixtures, Synth. Met. **154**, 237 (2005).
[41] E. Olejnik, C. Herzog-Ronen, Y. Eichen, and E. Ehrenfreund, Recombination kinetics of polarons in films of alkylator-sensing co-polymers, Synth. Met. **159**, 1024 (2009).
[42] T. Kobayashi, K. Kinoshita, T. Nagase, and H. Naito, Continuous-wave photoinduced absorption studies in polythiophene and fullerene blended thin films, Phys. Rev. B **83**, 035305 (2011).
[43] V. I. Krinichnyi, E. I. Yudanova, and N. N. Denisov, Light-induced EPR study of charge transfer in poly(3-hexylthiophene)/fullerene bulk heterojunction, J. Chem. Phys. **131**, 044515 (2009).

[44] E. L. Frankevich, A. A. Lymarev, I. Sokolik, F. E. Karasz, S. Blumstengel, R. H. Baughman, and H. H. Hörhold, Polaron-pair generation in poly(phenylene vinylenes), Phys. Rev. B **46**, 9320 (1992).

[45] G. Grancini, D. Polli, D. Fazzi, J. Cabanillas-Gonzalez, G. Cerullo, and G. Lanzani, Transient absorption imaging of P3HT:PCBM photovoltaic blend: Evidence For interfacial charge transfer state, J. Phys. Chem. Lett. **2**, 1099 (2011).